

Engineering ultra-strong Mg-Li-Al-based light-weight alloys from first principles

Okan K. Orhan¹ and Mauricio Ponga¹

¹*Department of Mechanical Engineering, University of British Columbia,
2054 - 6250 Applied Science Lane, Vancouver, BC, V6T 1Z4, Canada*

Light-weight alloys are essential pillars of transportation technologies. They also play a crucial role to achieve a more green and cost-effective aerospace technologies. Magnesium-lithium-aluminum (Mg-Li-Al) alloys are auspicious candidates due to their promising mechanical strengths at low densities. We herein present a systematic first-principles investigation of the Mg-Li-Al-based alloys to provide insights for designing ultra-strong light-weight alloys. Initial analysis indicates that the Mg-Li-Al mixtures are not thermally stabilized into random-solid solutions. Following this hint, the base-centered cubic (BCC)-based intermetallics of Mg, Li and Al are investigated for their thermal and elastic stabilities. Three simple figures of merits are used to further assess their mechanical strengths. The most-frequently observed intermetallics are used to predict the yield strength of the hetero-structures from the recent experimental works. The rule of mixing works reasonable well to predict the mechanical properties of complex structures starting from isolated intermetallics.

I. INTRODUCTION

Greener and cost-effective aerospace transportation has been an increasing concern to due to the commitment to cut carbon footprint in half by 2050 in civil aviation [1]. Furthermore, the rapidly growing military and commercial space exploration requires light materials which can provide protection against high-speed debris and micro-meteoroids collision [2, 3]. Both objectives highly rely on development of novel light-weight alloys (LWAs) with exceptional physical properties such as high strength, low density, fatigue durability, slow crack propagation, corrosion resistance and commercial advantages such as high workability, low-cost repairment/replacement and easy recycling/disposal [4].

Mg-Li alloys offer a good balance of strength and ductility [5], whilst AL-Li alloys have superior fracture toughness as they are commonly more brittle [6]. Mg-Li-Al alloys open up a large stoichiometric and phase space to explore LWAs with tunable mechanical properties. Introducing Al into the Mg-Li mixtures with small molar-fractions have been shown to improve specific strength while keeping the solid density low beyond the grain-refinement strengthening [7, 8]. Liu *et al.* [9] has

found that the Mg-14Li-1Al [weight % (wt%)], namely LA141, has three phases. The main phase is the BCC random solid solution (RSS) of Mg and Li, namely the β phase. The second predominant phase is the HCP RSS of Mg and Li, namely the α phase, which is embedded into the β matrix. Additionally, they have observed the BCC-based MgLiAl_2 , congregating in the α precipitates. It has been suggested that the α precipitates and MgLiAl_2 provides additional strengthening in this alloy.

Tang *et al.* [10] has found that on the Mg-11Li-3Al (wt%), namely LA113, has a $\alpha + \beta$ duplex structure with the $\text{D0}_3\text{-Mg}_3\text{Al}$ precipitates, semi-coherently forming in the β matrix. In this work, the $\text{D0}_3\text{-Mg}_3\text{Al}$ precipitates has been suggested as the predominant source of hardening, leading a Vickers hardness (H_V) of ~ 1.18 GPa at a low density of $\sim 1.4 \text{ g}\cdot\text{cm}^{-3}$. On the other hand, Xin *et al.* [11] has shown that the predominant hardening is due to the spinodal decomposition to the Al-rich zones in Mg-14Li-7Al (wt%), namely LA147, at the low ambient temperature. The Al-rich zones with a 4 nm diffusion zones are aligned in the elastically soft [100]-direction of the β phase. The spinodal-decomposition hardening leads to a Vickers hardness of ~ 1.47 GPa at a low density of $\sim 1.32 \text{ g}\cdot\text{cm}^{-3}$ in this sample. However, they have also noted that the Al-rich zones gradually transition to the $\text{D0}_3\text{-Mg}_3\text{Al}$ precipitates during the thermal aging.

In their recent experimental work, Li *et al.* [12] has investigated the phase formation and mechanical strength of the *nearly* equi-molar mixture of Mg, Li and Al. However, their sample becomes Mg-35Li-20Al (wt%) composition after treatment with a density of $1.68 \text{ g}\cdot\text{cm}^{-3}$. Similar to the previous work, their X-ray diffraction (XRD) measurement indicates the $\alpha + \beta$ duplex structure. XRD also predicts MgLiAl_2 , LiAl and Li_2Mg phases. The energy-dispersive X-ray spectroscopy (EDS) shows the Al-rich regions with the fish-bone micro-structures which are possibly embedded on the Mg-rich matrix. They have measured an exception ultimate strength of ~ 700 MPa and a Vickers hardness of 1.68 GPa.

Despite the rapidly growing experimental works, the current literature is limited to a handful of specific compositions. Furthermore, the nominal and actual chemical compositions may substantially differ after various post-treatments, aging, pollutants etc. With that challenge in mind, the first-principles simulations become crucial to gain insights when designing LWAs. In this work, we present a systematic first-principles investigation on the formation and mechanical properties of Mg-Li-Al-based LWAs. Our primary objective is to determine effects of intermetallic formation on the strength-density relation independently of complex sample preparations in the experimental works. The preliminary assessment indicates that the Mg-Li-Al mixtures do not form RSSs. This early finding and previous experimental works hint the formation of BCC-based intermetallics.

The thermal and elastic stability of the most-likely BBC-based intermetallics are investigated. First-principles figures of merits (FOMs) are used to predict ductility/brittleness, plasticity, and hardness of intermetallics. The rule of mixing is applied to the experimentally suggested mixtures to predict the accessible strength-density regions for the chosen Mg-Li-Al mixtures.

II. THEORETICAL AND COMPUTATIONAL METHODOLOGY

The Kohn-Sham formalism of density-functional theory (KS-DFT) [13, 14] using the semi-local exchange-correlation functionals [14–17] is the almost-ubiquitous approach for simulating the ground-state properties of quantum-mechanical systems. In this section, we will briefly introduce the theoretical concepts and their computational evaluation starting from the approximate KS-DFT electronic structures. Some common concepts are presented in the **Supplementary Material (SM)** to provide further details for the readers.

A. Figure of merit for random solid solution formation

Determining the likelihood of RSS formation is a quite challenging task as it requires a reasonable representation of statistical averaging of spatial disorderliness. The approximate KS-DFT has challenges when dealing spatially complex systems such as occupational disorderliness which requires simulations on a large number of super-cells to achieve a sufficient statistical representation. Virtual-crystal approximation (VCA) [18, 19] provides an expedient tool to assess single-phase multi-component solid at the disordered mean-field limit. In practice, VCA is an over-simplified approach by substituting the actual atoms with a single virtual atom represented by an linearly averaged pseudo-potential. Despite this, it has been shown to predict well equilibrium bulk properties and simple-phase transformations [20].

An expedient FOM for assessing the thermal stability is the heat of formation (H_F) given by [21]

$$H_F(\alpha, \beta, P) = E_{\text{Mg}_\alpha \text{Li}_\beta \text{Al}_\gamma}^P - [\alpha E_{\text{Mg}}^{\text{HCP}} + \beta E_{\text{Li}}^{\text{BCC}} + \gamma E_{\text{Al}}^{\text{FCC}}], \quad (1)$$

where $\gamma = 1 - \alpha - \beta$. $E_{\text{Mg}_\alpha \text{Li}_\beta \text{Al}_\gamma}^P$ is the total ground-state energy of the RSS of $\text{Mg}_\alpha \text{Li}_\beta \text{Al}_\gamma$ in the phase P . The phase P are chosen to be either HCP or BCC or face-centered cubic (FCC) as they are most likely crystal structures for simple metallic systems. $E_{\text{Mg}}^{\text{HCP}}$, $E_{\text{Li}}^{\text{BCC}}$ and $E_{\text{Al}}^{\text{FCC}}$ are the total

ground-state energies of the HCP Mg, BCC Li and FCC Al, respectively. RSS formation is only likely for $H_F < 0$.

B. Figures of merits for phase stability of intermetallics

A more robust and comprehensive stability assessment requires to assess thermal and elastic stability. A more accurate thermal-stability FOM is the mixing Gibbs free energy (GFE), given by [22]

$$G_{\text{mix}} = G_A - \sum_i^M c_i G_i, \quad (2)$$

where G_A , and G_i are the GFE of M -component and its i^{th} principle element with a molar fraction of c_i at their equilibrium volumes. For thermal stability, the mixing GFE is expected to be negative at a given temperature. For a non-magnetic and pristine solid, the GFE of a solid is the sum of the formation enthalpy ($H(V)$), the electronic ($F_{\text{el}}(V, T)$) and vibrational ($F_{\text{vib}}(V, T)$) Helmholtz free energies (see **SM** for details on how to approximately obtain these terms within the approximate KS-DFT). The Born-Huang-stability criteria [23, 24] provides the *necessary and sufficient* conditions for the elastic stability of a crystal (see **SM** for the reduced Born-Huang-stability criteria for the cubic and hexagonal symmetries). These criteria is indeed a special case of the thermal stability by ensuring that the GFE of an unstrained crystal is a minimum compared to its infinitesimally strained structures [25].

C. Figures of merits for mechanical properties

Calculating the mechanical properties of hetero-phased solids is a challenging task as there is large number of mechanism contributes to hardening and strength. However, the expedient FOMs can be used to assess workability, strength and hardness. Poisson's ratio and the Pugh ration are commonly used as FOMs for plasticity and ductility, respectively. Higher plasticity indicates well-workability, whilst lower ductility hints more mechanical strength. However, it is important to note that plasticity is prerequisite of ductility [26]. Hence, a critical balance between them is required for a well-workable and strong material. A critical minimum-value (CMV) of 0.25 for Poisson's ration [27], and a CMV of 1.75 for the Pugh ratio [28] are expected for plasticity, and ductility, respectively. The final FOM is the Vickers hardness(H_V) given by a semi-empirical relation of

$H_V = 0.151S$ [29] to the shear modulus (S). Moreover, H_V is approximately related to the yield strength (σ_y) with the semi-empirical formula $H_V \approx 3\sigma_y$ (in MPa units) [30].

These FOMs are directly related to the bulk and shear modulus which can be obtained via the Voigt-Reuss-Hill (VRH) averaging [31–33] of the second-order elastic tensor (see **SM** for further details). The second-elastic tensor can be calculated by performing a series of ground-state simulations on the infinitesimal-strained structures of a fully relaxed crystal, and using strain-stress relation in the linear-elastic region (see **SM** for the VHR averaging for the cubic and hexagonal symmetries).

D. An expedient approximation for mechanical properties of composite structures

The mechanical properties of a hetero-phased multi-component solid can be approximated by applying the rule of mixing to the bulk and shear modulus of its constituents. The approximate upper and lower bounds are given within the Voigt and Reuss averagings [31, 32], respectively, by

$$\mathbb{V} = \left(\sum_i^M f_i \mathbb{V}_i \right) \quad \text{and} \quad \mathbb{R} = \left(\sum_i^M \frac{f_i}{\mathbb{R}_i} \right)^{-1}, \quad (3)$$

where \mathbb{V}_i and \mathbb{R}_i are the Voigt and Reuss-averaged bulk or shear modulus of the i^{th} constituent with a volume fraction of f_i . The Voigt-Reuss-Hill (VHR) [33] is simply the arithmetic average of \mathbb{V}_i and \mathbb{R}_i (see **SM** for further details).

III. RESULTS AND DISCUSSION

We start with the preliminary assessment of the RSS-formation likelihood of $\text{Mg}_\beta\text{Li}_\alpha\text{Al}_\gamma$ alloys using VCA+KS-DFT. In Fig. 1 (left), the minimum H_F among the BCC, FCC and HCP phases of $\text{Mg}_\beta\text{Li}_\alpha\text{Al}_\gamma$ are shown. The positive H_F throughout the composition space indicates that Mg, Li and Al do not mix into single-phased, spatially disordered multi-component solids. Moreover, H_F are in the order of $10^1 - 10^2$ meV which is far too high to be possible compensated by the electronic, vibrational and configurational entropic contributions. This result can be further verified using the binary bulk metallic model [34] calculated via the Miedema’s model for pair-wise interaction [35]. In the right panel of Fig. 1, the minimum solid density (ρ) among the BCC, FCC and HCP phases of the $\text{Mg}_\beta\text{Li}_\alpha\text{Al}_\gamma$ are presented. The phases with the lowest ρ do not necessarily match with the phase with the lowest H_F .

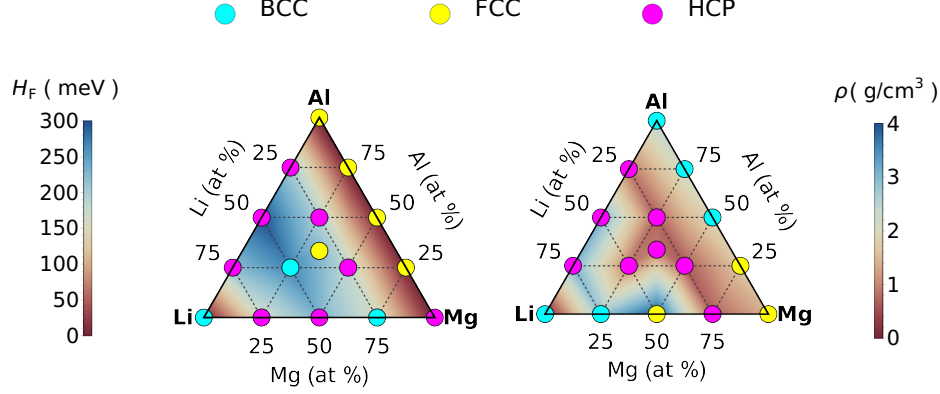


FIG. 1. Composition-dependence of the minimum heat of formation (H_F) and minimum solid density (ρ) among the BCC, FCC and HCP phases of the $\text{Mg}_\beta\text{Li}_\alpha\text{Al}_\gamma$ ($\gamma = 1 - \beta - \alpha$) RSS. Actual data points are marked by dots colored by their corresponding phases.

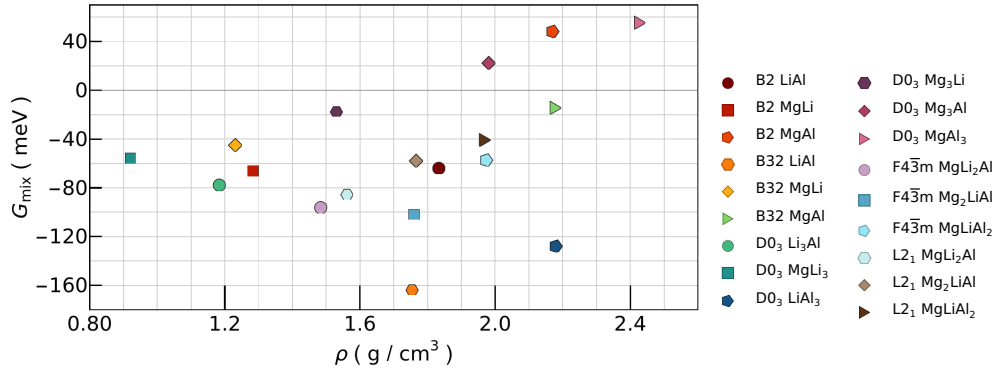


FIG. 2. Mixing Gibbs free energies of the simple body-centered-cubic-based intermetallics of Mg, Li and Al at 300 K using the Debye model for the vibrational Helmholtz energies.

A. Body-centered-cubic-based intermetallics

Since the $\text{Mg}_\beta\text{Li}_\alpha\text{Al}_\gamma$ mixtures are not expected to form RSSs, we shift our attention to their candidate BCC-based intermetallic (see **SM** for the templates of the most common BCC-based intermetallics). The BCC-based intermetallics are chosen as they are most commonly observed phases and most-likely candidates for high strength [10]. In Fig. 2, the mixing GFE of the isolated intermetallics are presented at 300 K. The mixing enthalpy, ΔH is equal to H_F by definition. H_V and the mixing vibrational Helmholtz energies (ΔF_{vib}) are the predominant terms in Eq. (2), whilst the electronic Helmholtz energies (ΔF_{el}) are negligible (see **SM-Fig. S1** for the individual contributions of each term).

In Fig. 2, the majority of the proposed intermetallics are thermally stable at the room temperature except B2 MgAl, D0₃ Mg₃Al and D0₃ MgAl₃. The B32 MgAl and D0₃ LiAl₃ phases are

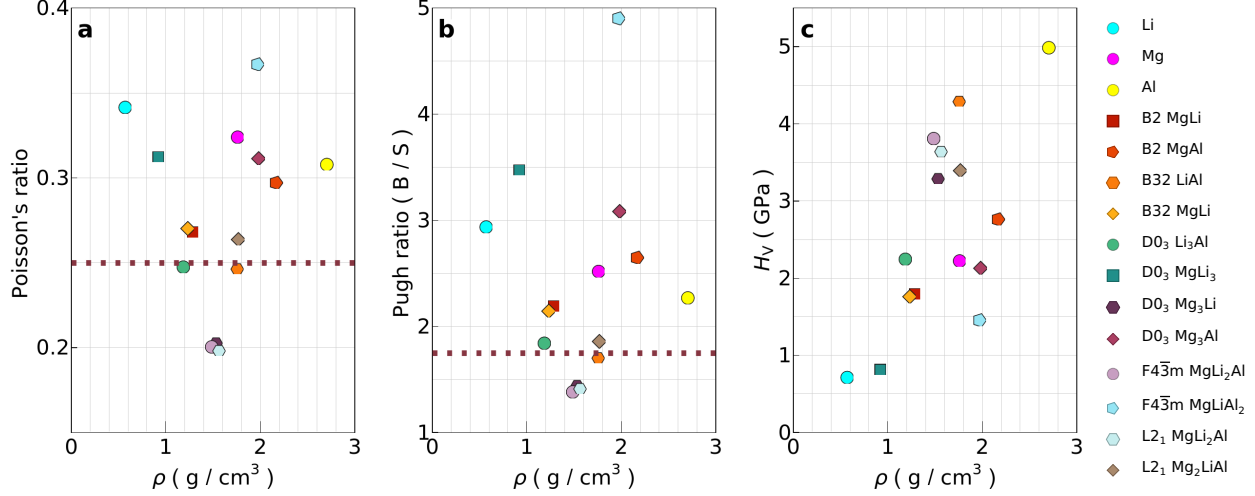


FIG. 3. Poisson's ratio, Pugh ratio and Vickers hardness of the elastically stable intermetallics of Mg, Li and Al.

thermally stabilized by ΔF_{vib} , compensating their positive H_F . ΔF_{el} of the intermetallics mostly work against the thermal stability; however, they are negligible compared to H_F and ΔF_{vib} . In general, ΔF_{vib} works against thermal stability at lower densities whilst they improve thermal stability at higher densities. Among the thermally unstable phases, the D0₃ MgAl₃ need further attention due to its particular importance. Although the isolated D0₃ Mg₃Al phase is not thermally stable, Tang *et al.* has shown that it reaches to a meta-stable phase due to its semi-coherent precipitation with the BCC Li matrix [10].

In Fig. 3, the three FOMs for the critical mechanical properties are shown for the elastically stable intermetallics alongside the elemental cases. The elemental cases behave as expected for which the BCC Li exhibits the lowest strength and hardness with the best workability and the FCC Al exhibits the highest strength and hardness with the worst workability among Mg, Li and Al. MgLiAl₂ has the highest Poisson's and Pugh ratios, indicating the lowest strength among the available intermetallics. This contradicts with the prediction of Liu *et al.* [9] where they have claimed that MgLiAl₂ can be an additional source of hardening. Moreover, the F4 $\bar{3}$ m MgLiAl₂ phase is elastically stable while the more-commonly suggested L2₁ MgLiAl₂ phase is not. This may suggest that MgLiAl₂ is most-likely only meta-stable and decompose to lower-ordered intermetallics and/or the elemental phases. Indeed, the previous work by Levinson and McPherson [36] have predicted MgLi₂Al phase rather than MgLiAl₂. The both L2₁ and F4 $\bar{3}$ m phases of MgLi₂Al exhibit quite promising in terms of strength and hardness. Similarly, the isolated D0₃ Mg₃Al does not show any exceptional strength or hardness. It may be a hint that D0₃ Mg₃Al leads to exceptional

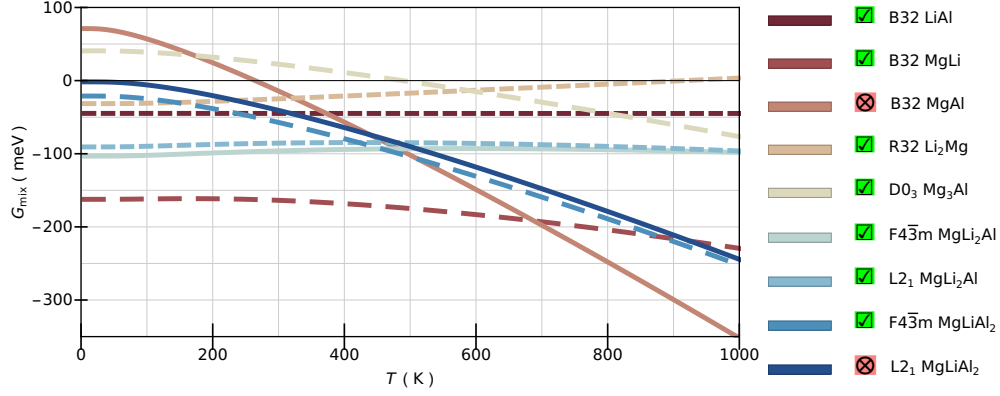


FIG. 4. Temperature-dependent mixing Gibbs free energies of the most-frequently observed intermetallics in Mg-Li-Al mixtures. The elastically stable phases are marked with the green check-box, otherwise with the red cross-box.

hardening (as suggested by Tang *et al.* [10]) due to its semi-coherent precipitation on the Li matrix. By doing so, it may lead to exceptional hardening through the precipitation hardening rather than its intrinsic mechanical superiority.

B. Assessment of hardening mechanisms

We select the subset of intermetallics which have been frequently predicted in the previous experimental works to further gain insight on hardening mechanics. In Fig. 4, the temperature-dependent mixing GFE of the most-frequently appearing phases are shown alongside their elastic-stability test results. Among them, the B32 MgAl and D0₃ Mg₃Al phases have positive H_F ($G_{\text{mix}}(T = 0) = H_F$); however, their G_{mix} decrease with the increasing temperature. B32 MgAl and D0₃ Mg₃Al become thermally stable at around ~ 265 K and ~ 490 K, respectively. On the other hand, the R32 Li₂Mg is the only phase with a significantly increasing G_{mix} when the temperature rises. It is thermally stable at the lower temperatures; however, it becomes unstable at around ~ 920 K. In the legend of Fig. 4, the results of the elastic-stability tests according to the Born-Huang-stability criteria are shown by the colored boxes for which the green check-box and the red cross-box represent pass and fail, respectively. The isolated crystals of the selected phases are elastically stable except the B32 MgAl and L2₁ MgLiAl₂ phases. In particular, the L2₁ MgLiAl₂ phase is concerning as it is often the assigned symmetry in the XRD measurements. However, the F4 $\bar{3}$ m MgLiAl₂ phase is elastically stable with a similar $G_{\text{mix}}(T)$ to the L2₁ MgLiAl₂ phase. The XRD measurements may not be have enough resolution to distinguish these two symmetries.

In Fig. 5 (left), the strength-density profiles of the most-frequently appearing intermetallics

in the Mg-Li-Al mixtures are shown alongside the most recent experimental predictions on the hetero-structures. Using B32 MgLi, which has $\sigma_y = 0.59$ GPa and $\rho = 1.23 \text{ g}\cdot\text{cm}^{-3}$, as the reference system, the intermetallics with Al contents such as D0₃ Mg₃Al and F43m MgLiAl₂ are not favorable due to significantly higher density with comparable strengths. On the other hand, the MgLi₂Al intermetallics exhibits remarkable strengths in between of $\sim 1.2 - 1.3$ GPa with a slightly higher density of $\sim 1.5 \text{ g}\cdot\text{cm}^{-3}$.

In terms of strength, the sample with an average composition of Mg₃₀Li₄₈Al₂₂ from Ref.12 is superior at the expense of a higher density compared the samples with average compositions of Mg₆₆Li₃₀Al₄ and Mg₄₅Li₃₀Al₂₅ from Refs. 10 and 11, respectively. In the right panel of Fig. 5, the estimated strength-density regions, \mathcal{R}_1 and \mathcal{R}_2 are calculated using the rule of mixing for

$$\begin{aligned} \mathcal{R}_1 &: \text{MgLiAl} \\ \mathcal{R}_2 &: \text{Mg}_{30}\text{Li}_{48}\text{Al}_{22} \\ &\downarrow \\ c_1\text{Li} + c_2\text{Mg} + c_3\text{LiAl} + c_4\text{Li}_2\text{Mg} + c_5\text{MgLiAl}_2 \end{aligned}$$

Similarly, the strength-density curve, \mathcal{L}_1 is calculated for

$$\mathcal{L}_1 : \text{Mg}_{70-x}\text{Li}_{30}\text{Al}_x \rightarrow 30\text{Li} + (70 - 4x)\text{Mg} + x\text{Mg}_3\text{Al}.$$

The region \mathcal{R}_1 represent an hypothetical MgLiAl composition forming the hetero-structures of the intermetallics from Ref. 12. \mathcal{R}_1 indicates that the MgLiAl composition may provide significant strengths at reasonably low densities. The justification of the simple rule of mixing is the region \mathcal{R}_2 where the experimentally measured composition of Mg₃₀Li₄₈Al₂₂ is targeted. The experimental measurement on this composition is located nearly at the center of the estimate strength-density region. The curve \mathcal{L}_1 is inspired by the work in Refs. 10 and 11 where the effects of increasing Al content and resulting D0₃ Mg₃Al precipitation has been investigated. On remarkable trend is that the increasing Al content indeed reduces the density due to increasing volume fraction of D0₃ Mg₃Al which has a smaller volume per atom compared to HCP Mg. The calculate \mathcal{L}_1 overestimates the strength of Mg₆₆Li₃₀Al₄; however, it predict well the strength of Mg₄₅Li₃₀Al₂₅. This is quite promising that the simple rule of mixing can be used as a predictive model to estimate the strength-density profiles of Mg-Li-Al hetero-structures starting from the simple Mg-Li-Al intermetallics. Moreover, the promising hetero-structures can be architected using the promising intermetallics

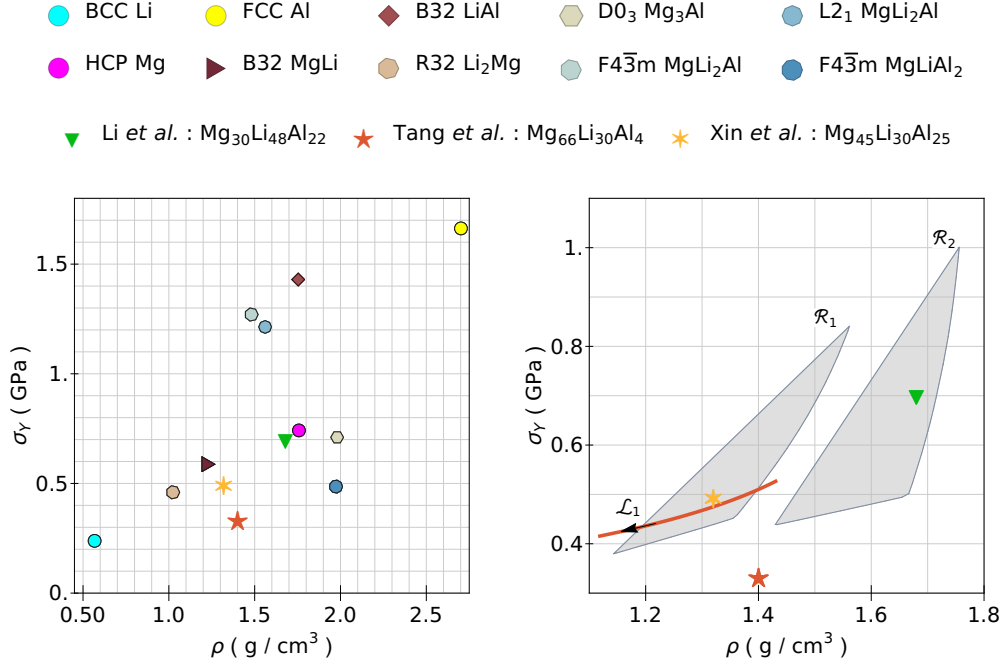


FIG. 5. Approximate yield strength of the most-frequent intermetallics in the Mg-Li-Al mixtures alongside the experimental values by Li *et al* for $\text{Mg}_{30}\text{Li}_{48}\text{Al}_{22}$ [12], Tang *et al.* for $\text{Mg}_{66}\text{Li}_{30}\text{Al}_4$ [10] and Xin *et al.* for $\text{Mg}_{45}\text{Li}_{30}\text{Al}_{25}$ [11]. Two strength-density regions, \mathcal{R}_1 and \mathcal{R}_2 are calculated by applying the rule of mixing to Li, Mg, B32 LiAl, R32 Li_2Mg and $\text{F}\bar{4}3\text{m}$ MgLiAl_2 (phases observed in the works of Li *et al*) for the MgLiAl and $\text{Mg}_{30}\text{Li}_{48}\text{Al}_{22}$ compositions. The strength-density curve, \mathcal{L}_1 is obtained by applying the rule of mixing to Li, Mg, $\text{D}0_3$ Mg_3Al for the $\text{Mg}_{70-x}\text{Li}_{30}\text{Al}_x$.

IV. CONCLUSION

In this work, we presented a systematic first-principles investigation of formations and strength-density profiles of the Mg-Li-Al LWAs. It was expediently shown by applying VCA that the Mg-Li-Al mixtures do not form RSSs. Following this, the thermal and elastic stabilities of the BCC-based intermetallics were assessed and the mechanical properties of the elastically stable intermetallics were studied for their possible hardening contributions to the hetero-structures. Despite its frequent appearance in the experimental measurements on the Mg-Li-Al hetero-structures, MgLiAl_2 does not offer any significant hardening compared the conventional Mg-Li alloys such as B32 MgLi. On the other hand, the MgLi_2Al intermetallics can be quite promising hardening source while keeping density low. The simple rule of mixing using the isolated intermetallics works remarkable well when estimating the mechanical strength of the complex hetero-structures. It was shown that it

can be used to engineer the strength-density profiles of complex structures.

ACKNOWLEDGMENT

We acknowledge the support from the Natural Sciences and Engineering Research Council of Canada (NSERC) through the Discovery Grant under Award Application Number RGPIN-2016-06114, and the New Frontiers in Research Fund (NFRFE-2019-01095). This research was supported in part through computational resources and services provided by Advanced Research Computing at the University of British Columbia.

-
- [1] M. Marino and R. Sabatini, Advanced lightweight aircraft design configurations for green operations (Practical Responses to Climate Change, 2014).
 - [2] M. A. Tunes, L. Stemper, G. Greaves, P. J. Uggowitzer, and S. Pogatscher, Metal alloy space materials: Prototypic lightweight alloy design for stellar-radiation environments (adv. sci. 22/2020), *Advanced Science* **7**, 2070126 (2020).
 - [3] H. Jones, The recent large reduction in space launch cost (48th International Conference on Environmental Systems, 2018).
 - [4] L. Zhu, N. Li, and P. Childs, Light-weighting in aerospace component and system design, *Propulsion and Power Research* **7**, 103 (2018).
 - [5] T. W. Cain and J. P. Labukas, The development of β phase mg–li alloys for ultralight corrosion resistant applications, *npj Materials Degradation* **4**, 17 (2020).
 - [6] R. J. Rioja and J. Liu, The evolution of al–li base products for aerospace and space applications, *Metallurgical and Materials Transactions A* **43**, 3325 (2012).
 - [7] P. Wang, Y. Du, and S. Liu, Thermodynamic optimization of the li–mg and al–li–mg systems, *Calphad* **35**, 523 (2011), world Round Robin Seminar 2010.
 - [8] P. Fei, Z. Qu, and R. Wu, Microstructure and hardness of mg–9li–6al–xla (x=0, 2, 5) alloys during solid solution treatment, *Materials Science and Engineering: A* **625**, 169 (2015).
 - [9] T. Liu, S. Wu, S. Li, and P. Li, Microstructure evolution of mg–14process of equal channel angular pressing, *Materials Science and Engineering: A* **460-461**, 499 (2007).
 - [10] S. Tang, T. Xin, W. Xu, D. Miskovic, G. Sha, Z. Quadir, S. Ringer, K. Nomoto, N. Birbilis, and M. Ferry, Precipitation strengthening in an ultralight magnesium alloy, *Nature Communications* **10**, 1003 (2019).
 - [11] T. Xin, Y. Zhao, R. Mahjoub, J. Jiang, A. Yadav, K. Nomoto, R. Niu, S. Tang, F. Ji, Z. Quadir, D. Miskovic, J. Daniels, W. Xu, X. Liao, L.-Q. Chen, K. Hagihara, X. Li, S. Ringer, and M. Ferry,

- Ultrahigh specific strength in a magnesium alloy strengthened by spinodal decomposition, *Science Advances* **7**, 10.1126/sciadv.abf3039 (2021).
- [12] H. Li, C. Shao, D. F. Rojas, M. Ponga, and J. D. Hogan, Micro-hardness and strain-rate-dependent compressive response of an ultra-light-weight mg-li-al alloy, *Journal of Alloys and Compounds* **890**, 161703 (2022).
 - [13] P. Hohenberg and W. Kohn, Inhomogeneous electron gas, *Phys. Rev.* **136**, B864 (1964).
 - [14] W. Kohn and L. J. Sham, Self-consistent equations including exchange and correlation effects, *Phys. Rev.* **140**, A1133 (1965).
 - [15] D. C. Langreth and J. P. Perdew, Theory of nonuniform electronic systems. i. analysis of the gradient approximation and a generalization that works, *Phys. Rev. B* **21**, 5469 (1980).
 - [16] J. P. Perdew, Density-functional approximation for the correlation energy of the inhomogeneous electron gas, *Phys. Rev. B* **33**, 8822 (1986).
 - [17] J. P. Perdew, J. A. Chevary, S. H. Vosko, K. A. Jackson, M. R. Pederson, D. J. Singh, and C. Fiolhais, Atoms, molecules, solids, and surfaces: Applications of the generalized gradient approximation for exchange and correlation, *Phys. Rev. B* **46**, 6671 (1992).
 - [18] L. Nordheim, Zur elektronentheorie der metalle. i, *Annalen der Physik* **401**, 607 (1900).
 - [19] L. Bellaiche and D. Vanderbilt, Virtual crystal approximation revisited: Application to dielectric and piezoelectric properties of perovskites, *Phys. Rev. B* **61**, 7877 (2000).
 - [20] F. Tian, A review of solid-solution models of high-entropy alloys based on ab initio calculations, *Frontiers in Materials* **4**, 36 (2017).
 - [21] H. Zhang, S. Shang, J. E. Saal, A. Saengdeejing, Y. Wang, L.-Q. Chen, and Z.-K. Liu, Enthalpies of formation of magnesium compounds from first-principles calculations, *Intermetallics* **17**, 878 (2009).
 - [22] A. Fernández-Caballero, M. Fedorov, J. S. Wróbel, P. M. Mummery, and D. Nguyen-Manh, Configurational entropy in multicomponent alloys: Matrix formulation from ab initio based hamiltonian and application to the fcc cr-fe-mn-ni system, *Entropy* **21**, 10.3390/e21010068 (2019).
 - [23] M. Born and K. Huang, *Dynamical theory of crystal lattices*, Oxford classic texts in the physical sciences (Clarendon Press, Oxford, 1954).
 - [24] F. Mouhat and F. m. c.-X. Coudert, Necessary and sufficient elastic stability conditions in various crystal systems, *Phys. Rev. B* **90**, 224104 (2014).
 - [25] H. Demarest, R. Ota, and O. Anderson, Prediction of high pressure phase transitions by elastic constant data, in *High-Pressure Research*, edited by M. H. Manghnani and S.-I. Akimoto (Academic Press, 1977) pp. 281–301.
 - [26] Y. Zhu and X. Wu, Ductility and plasticity of nanostructured metals: differences and issues, *Materials Today Nano* **2**, 15 (2018).
 - [27] S. Pugh, Xcii. relations between the elastic moduli and the plastic properties of polycrystalline pure metals, *The London, Edinburgh, and Dublin Philosophical Magazine and Journal of Science* **45**, 823 (1954).

- [28] S. Boucetta, Theoretical study of elastic, mechanical and thermodynamic properties of mgrh inter-metallic compound, *Journal of Magnesium and Alloys* **2**, 59 (2014).
- [29] D. M. Teter, Computational alchemy: The search for new superhard materials, *MRS Bulletin* **23**, 22–27 (1998).
- [30] M. Tiryakioğlu, On the relationship between vickers hardness and yield stress in al–zn–mg–cu alloys, *Materials Science and Engineering: A* **633**, 17 (2015).
- [31] W. Voigt, Ueber die beziehung zwischen den beiden elasticitätsconstanten isotroper körper, *Annalen der Physik* **274**, 573 (1889).
- [32] A. Reuss, Berechnung der fließgrenze von mischkristallen auf grund der plastizitätsbedingung für einkristalle ., *ZAMM - Journal of Applied Mathematics and Mechanics / Zeitschrift für Angewandte Mathematik und Mechanik* **9**, 49 (1929).
- [33] R. Hill, The elastic behaviour of a crystalline aggregate, *Proceedings of the Physical Society. Section A* **65**, 349 (1952).
- [34] K. M. Youssef, A. J. Zaddach, C. Niu, D. L. Irving, and C. C. Koch, A novel low-density, high-hardness, high-entropy alloy with close-packed single-phase nanocrystalline structures, *Materials Research Letters* **3**, 95 (2015).
- [35] A. Takeuchi and A. Inoue, Classification of bulk metallic glasses by atomic size difference, heat of mixing and period of constituent elements and its application to characterization of the main alloying element, *MATERIALS TRANSACTIONS* **46**, 2817 (2005).
- [36] D. Levinson and D. McPherson, Phase relations in magnesium-lithium-aluminum alloys, *Transactions of the American Society for Metals* **48**, 689 (1956).

Supplementary Materials

“Engineering ultra-strong Mg-Li-Al-based light-weight alloys from first principles”

Okan K. Orhan¹ and Mauricio Ponga¹

¹*Department of Mechanical Engineering, University of British Columbia,
2054 - 6250 Applied Science Lane, Vancouver, BC, V6T 1Z4, Canada*

GIBBS FREE ENERGY

The Gibbs free energy (GFE) of a non-magnetic, and pristine solid is given by

$$G(V, T) = H(V) + F_{\text{el}}(V, T) + F_{\text{vib}}(V, T), \quad (\text{S1})$$

where $H(V)$ is the formation enthalpy, $F_{\text{el}}(V, T)$ and $F_{\text{vib}}(V, T)$ are the electronic and vibrational Helmholtz free energies, respectively.

At the equilibrium volume, $H(V)$ is simply equal to the internal energy. Within the approximate KS-DFT, the total energy (E_0) is not physically meaningful [S1]. However, E_0 is still useful to approximate the mixing enthalpies when the atomic pseudo-potentials are used consistently.

The electronic Helmholtz free energy is given for metallic systems by [S2–S4]

$$F_{\text{el}} = \left(\int dE N(E, V) f E - \int^{E_F} dE N(E, V) E \right) + T \left(k_B \int dE N(E, V) [f \ln(f) + (1 - f) \ln(1 - f)] \right), \quad (\text{S2})$$

where k_B is the Boltzmann constant, $N(E, V)$ is the electron density of states (DOS), $f = f(E, E_F, T)$ is the Fermi-Dirac distribution function around the Fermi level with the Fermi energy, E_F .

The simplest approach to obtain the vibrational Helmholtz free energy is within the Debye model, given by [S5, S6]

$$F_{\text{vib}}^{\text{D}} = \frac{9}{8} k_B \Theta_D + k_B T \left\{ 3 \ln \left[1 - e^{-\frac{\Theta_D}{T}} \right] + D \left[\frac{\Theta_D}{T} \right] \right\}, \quad (\text{S3})$$

where Θ_D is the Debye temperature, and

$$D(x) = \frac{3}{x^3} \int_0^x du \frac{u^3}{e^u - 1}.$$

The Debye temperature is approximately given by [S7]

$$\Theta_D = \frac{h}{k_B} \left[\frac{3}{4\pi} \frac{N}{V} \right]^{1/3} v_s, \quad (\text{S4})$$

where N is the number of atoms in the unit cell and v_s is the average sound velocity. The average sound velocity, v_s can be determined by solving the Christoffel equation in each direction [S8].

THE BORN-HUANG-STABILITY CRITERIA FOR THE CUBIC AND HEXAGONAL SYMMETRIES

The necessary and sufficient conditions for the elastic stability of cubic systems are given by [S9]

$$c_{11}c_{12} > 0, \quad c_{11} + 2c_{12} > 0 \text{ and } c_{44} > 0 \quad (\text{S5})$$

where c_{ij} are the elements of the second-order elastic tensor \mathbb{C} .

In the case of the hexagonal symmetry, the necessary and sufficient conditions are

$$c_{11} > |c_{12}|, \quad c_{33} (c_{11} + c_{12}) > 2c_{13}^2 \text{ and } c_{44} > 0. \quad (\text{S6})$$

In the case of the rhombohedral symmetry, the necessary and sufficient conditions are

$$\begin{aligned} c_{11} > |c_{12}|, \quad c_{33} (c_{11} + c_{12}) > 2c_{13}^2, \\ c_{44}c_{66} > c_{14}^2 \text{ and } c_{44} > 0. \end{aligned} \quad (\text{S7})$$

ELASTIC CONSTANTS OF THE CUBIC AND HEXAGONAL SYSTEMS

The Voigt-Reuss-Hill (VHR) [S10] averaged bulk (B) and shear (S) modulus are given by

$$B_{\text{VHR}} = \frac{B_V + B_R}{2}, \quad \text{and} \quad S_{\text{VHR}} = \frac{S_V + S_R}{2}, \quad (\text{S8})$$

where the sub-indices V and R represent the Voigt and Reuss averagings [S11, S12] which provide the upper and lower bounds, respectively. The Voigt- and Reuss-averaged bulk and shear modulus for cubic systems are given by [S13]

$$\begin{aligned} B_V = B_R &= \frac{c_{11} + 2c_{12}}{3}, \\ S_V &= \frac{c_{11} - c_{12} + 3c_{44}}{5}, \quad \text{and} \quad S_R = \frac{5(c_{11} - c_{12})c_{44}}{3c_{11} - 3c_{12} + 4c_{44}}. \end{aligned} \quad (\text{S9})$$

Similarly, the Voigt- and Ruess-averaged bulk and shear modulus for hexagonal systems are given by [S14]

$$\begin{aligned} B_V &= \frac{2(c_{11} + c_{12} + 0.5c_{33} + 2c_{13})}{9}, \quad \text{and} \quad B_R = \frac{1}{3\alpha + 6\beta} \\ S_V &= \frac{7c_{11} - 5c_{12} + 12c_{44} + 2c_{33} - 4c_{13}}{30}, \quad \text{and} \\ S_R &= \frac{5}{4\alpha - 4\beta + 3\lambda}, \end{aligned} \quad (\text{S10})$$

where $3\alpha = s_{11} + s_{11} + s_{33}$, $3\beta = s_{23} + s_{31} + s_{12}$, and $3\lambda = s_{44} + s_{55} + s_{66}$. s_{ij} is elements of the elastic compliances matrix given by $\mathbb{S} = \mathbb{C}^{-1}$. Then, Young's modulus (Y) and the Poisson ratio (ν_P) are given in terms of B and S by

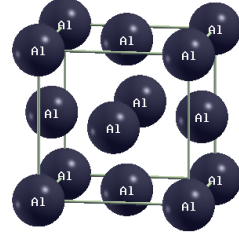
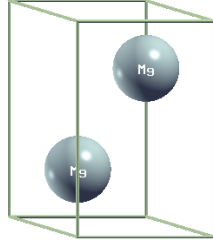
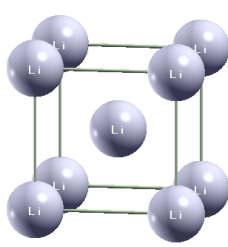
$$Y = \frac{9BS}{3B + S}, \quad \text{and} \quad \nu_P = \frac{3B - 2S}{6B + 2S}. \quad (\text{S11})$$

COMPUTATIONAL DETAILS

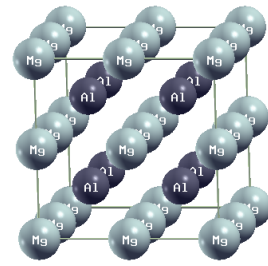
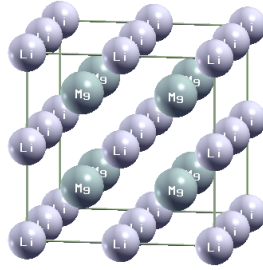
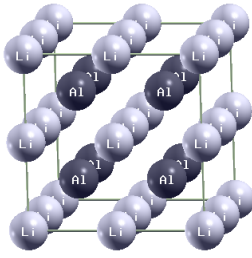
The SG15 optimized norm-conserving Vanderbilt scalar-relativistic pseudo-potentials [S15, S16] using the Perdew-Burke-Ernzerhof exchange-correlation functional [S17–S19] were used for the Mg, Li, and Al atomic pseudo-potentials. Initial crystallographic information of the stable phases of Mg, Li, and Al were extracted from Ref. S20. Initial crystallographic information were obtained by substituting the virtual atoms for Mg, Li, and Al during random solid solution simulations at the disordered mean-field limit. The initial crystal structures for the available body-centered cubic (BCC) intermetallics were constructed by using the generic templates, shown in Fig. S-1.

Variable-cell geometry optimizations were performed using the Quantum ESPRESSO (QE) software [S21, S22] with a 150 Ry kinetic-energy cutoff, a Marzari-Vanderbilt cold-smearing [S23] equivalent to 300 K, and a $12 \times 12 \times 12$ Monkhorst-Pack-equivalent [S24] uniform Brillouin zone with a 10^{-7} Ry total-energy, and 10^{-6} Ry/ a_0 total force convergence and 10^{-10} self-consistency

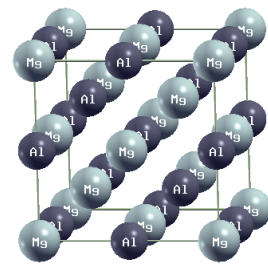
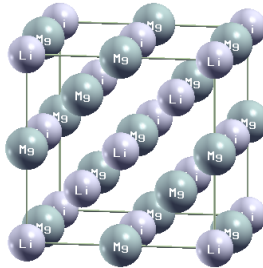
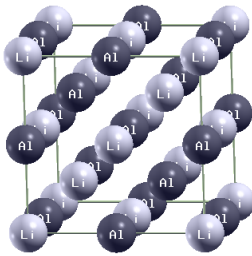
thresholds. Thermodynamic quantities, the elastic properties, and the phonon dispersion were calculated using the *"thermo_pw"* package [S25] within the QE software with a commonly converged kinetic-energy cutoff of 100 Ry on a $12 \times 12 \times 12$ shifted Monkhorst-Pack-equivalent uniform Brillouin zone.



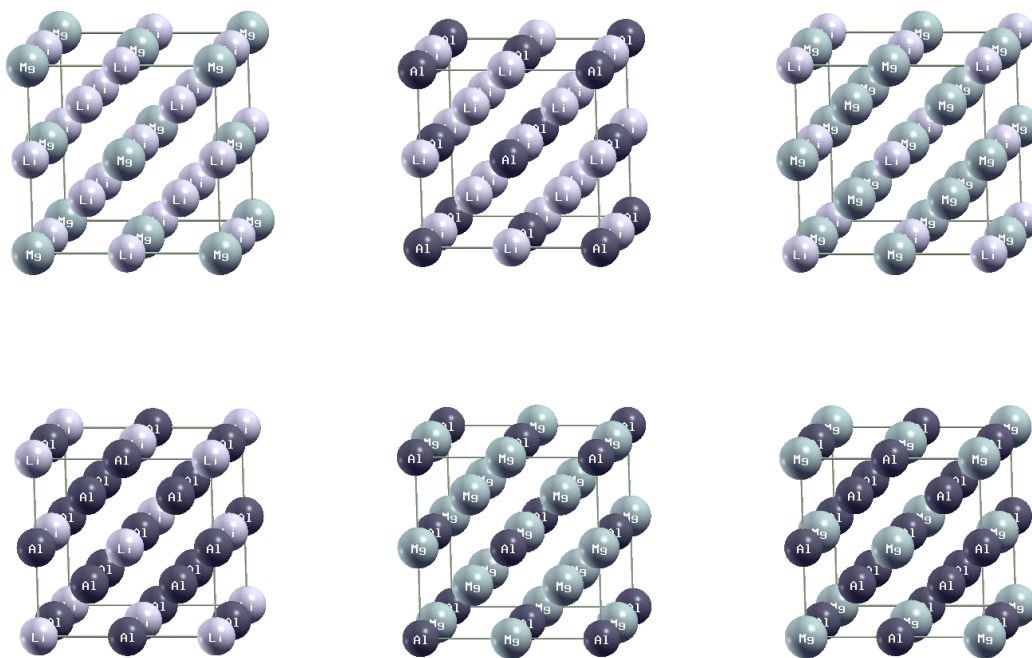
(a) Elemental metals



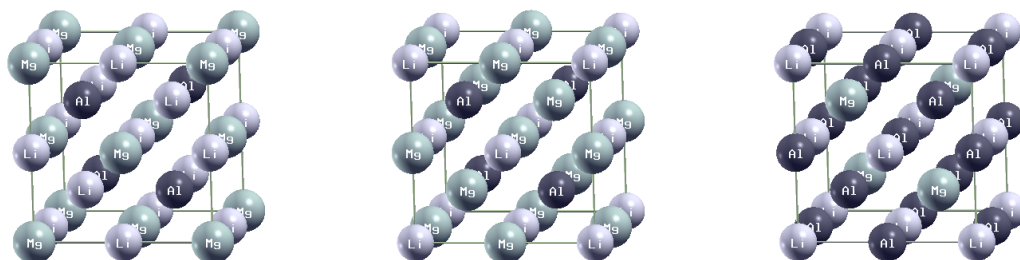
(b) B2 ordered structure *AB* alloys



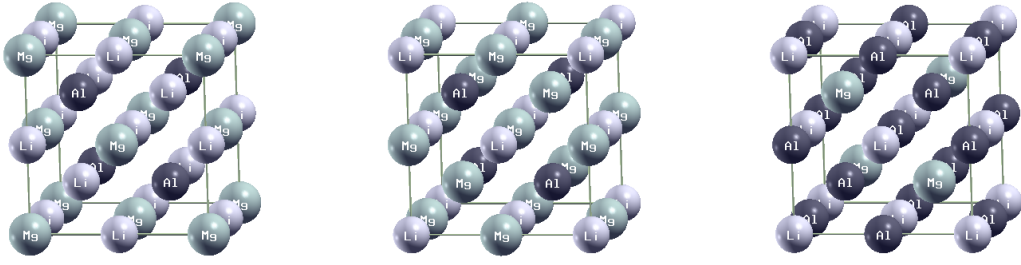
(c) B32 ordered structure *AB* alloys



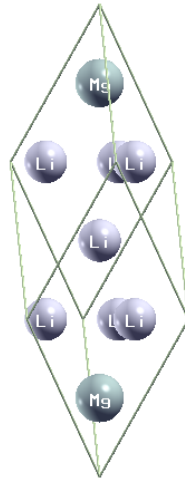
(d) $D0_3$ ordered structure A_3B alloys



(e) $F4_3m$ ordered structure A_2BC alloys



(f) $F\bar{4}3m$ ordered structure A_2BC alloys



(g) R32 Li_2Mg

FIG. S-1. Crystal structures of Mg, Li, and Al intermetallics.

TEMPERATURE-DEPENDENCE OF FREE ENERGIES OF THE BODY-CENTERED-CUBIC INTERMETALLICS

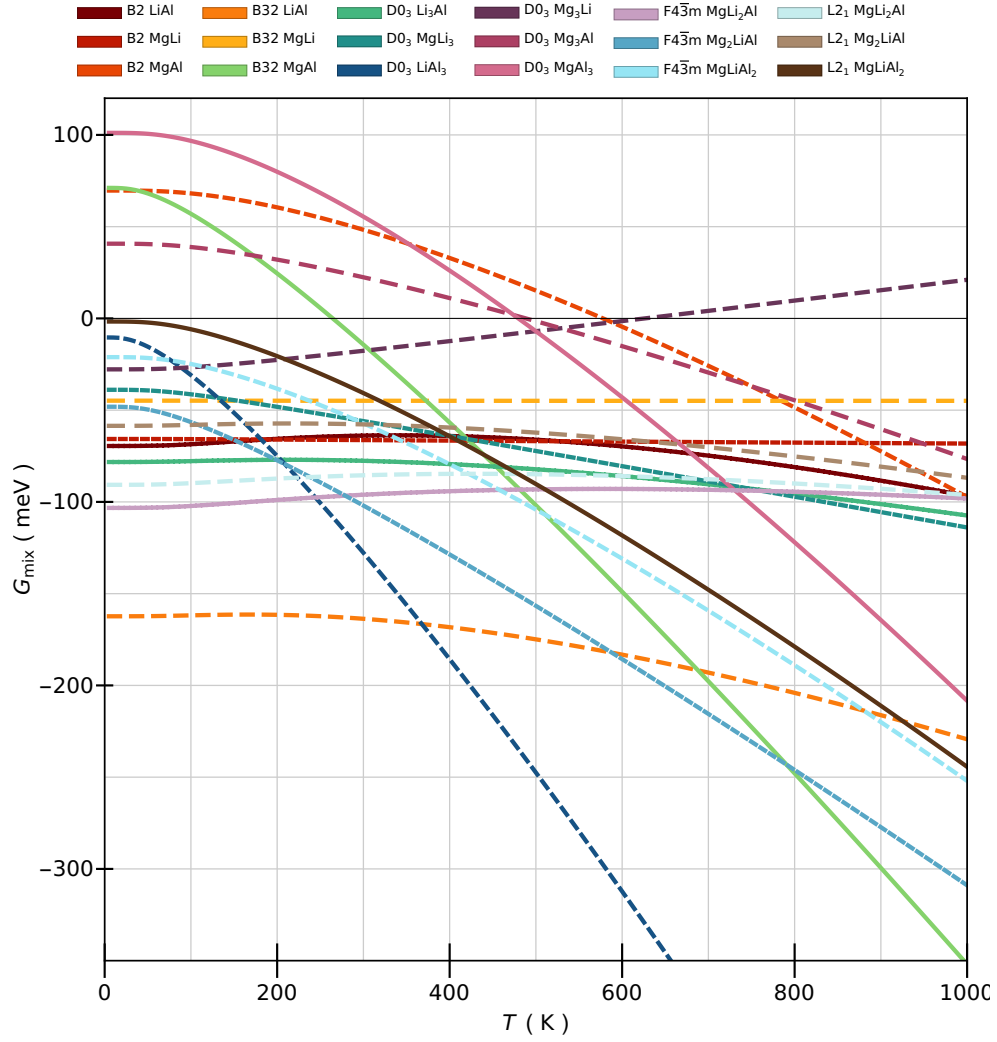


FIG. S0. Temperature dependence of the mixing Gibbs free energies of the body-centered-cubic-based intermetallic of Mg, Li and Al. The predominant terms are the vibrational Helmholtz energies in determining the temperature-dependent trends. The vibrational Helmholtz energies are calculated within the Debye model.

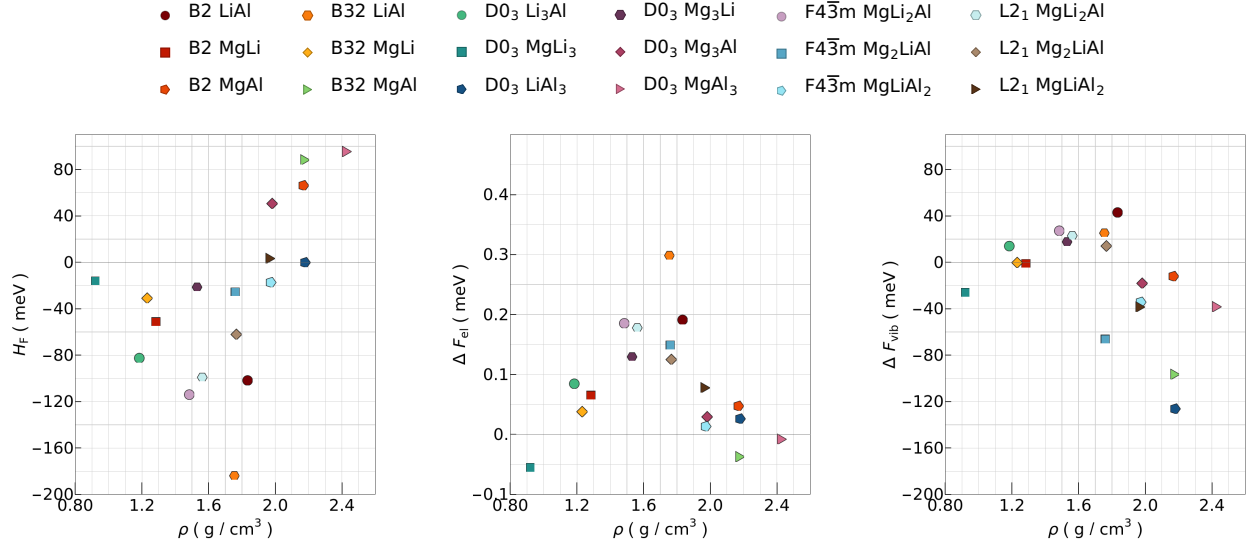


FIG. S1. The three main contribution to the mixing Gibbs free energies at 300 K.

-
- [S1] V. Heine, The pseudopotential concept (Academic Press, 1970) pp. 1–36.
- [S2] Y. Wang, Z.-K. Liu, and L.-Q. Chen, Thermodynamic properties of Al, Ni, NiAl, and Ni₃Al from first-principles calculations, *Acta Materialia* **52**, 2665 (2004).
- [S3] L. Landau and E. Lifshitz, Statistical physics (Pergamon Press, Headington Hill Hall, Oxford, OX3 0BW England, 1980) Chap. 5, pp. 158–168, 3rd ed.
- [S4] F. Tian, A review of solid-solution models of high-entropy alloys based on ab initio calculations, *Frontiers in Materials* **4**, 36 (2017).
- [S5] O. L. Anderson, Physical acoustics, Vol. III. Part B. Lattice Dynamics. Ed. Mason WP–New York and London **62** (1965).
- [S6] S.-L. Shang, Y. Wang, D. Kim, and Z.-K. Liu, First-principles thermodynamics from phonon and debye model: Application to ni and ni3al, *Computational Materials Science* **47**, 1040 (2010).
- [S7] O. L. Anderson, A simplified method for calculating the debye temperature from elastic constants, *Journal of Physics and Chemistry of Solids* **24**, 909 (1963).
- [S8] J. W. Jaeken and S. Cottenier, Solving the christoffel equation: Phase and group velocities, *Computer Physics Communications* **207**, 445 (2016).
- [S9] F. Mouhat and F. m. c.-X. Coudert, Necessary and sufficient elastic stability conditions in various crystal systems, *Phys. Rev. B* **90**, 224104 (2014).
- [S10] R. Hill, The elastic behaviour of a crystalline aggregate, *Proceedings of the Physical Society. Section A* **65**, 349 (1952).
- [S11] W. Voigt, Ueber die beziehung zwischen den beiden elasticittsconstanten isotroper krper, *Annalen der*

- Physik **274**, 573 (1889).
- [S12] A. Reuss, Berechnung der fliegrenze von mischkristallen auf grund der plastizittsbedingung fr einkristalle ., *ZAMM - Journal of Applied Mathematics and Mechanics / Zeitschrift fr Angewandte Mathematik und Mechanik* **9**, 49 (1929).
 - [S13] P. Hao, P. Chen, L. Deng, F. Li, J. Yi, D. opu, J. Eckert, J. Tao, Y. Liu, and R. Bao, Anisotropic elastic and thermodynamic properties of the hcp-titanium and the fcc-titanium structure under different pressures, *Journal of Materials Research and Technology* **9**, 3488 (2020).
 - [S14] D. Tromans, Elastic anisotropy of hcp metal crystals and polycrystals, *Int. J. Res. Rev. Appl. Sci* **6**, 462 (2011).
 - [S15] D. R. Hamann, Optimized norm-conserving vanderbilt pseudopotentials, *Phys. Rev. B* **88**, 085117 (2013).
 - [S16] M. Schlipf and F. Gygi, Optimization algorithm for the generation of oncv pseudopotentials, *Computer Physics Communications* **196**, 36 (2015).
 - [S17] D. R. Hamann, M. Schlüter, and C. Chiang, Norm-conserving pseudopotentials, *Phys. Rev. Lett.* **43**, 1494 (1979).
 - [S18] G. P. Kerker, Non-singular atomic pseudopotentials for solid state applications, *Journal of Physics C: Solid State Physics* **13**, L189 (1980).
 - [S19] D. R. Hamann, Generalized norm-conserving pseudopotentials, *Phys. Rev. B* **40**, 2980 (1989).
 - [S20] A. Jain, S. P. Ong, G. Hautier, W. Chen, W. D. Richards, S. Dacek, S. Cholia, D. Gunter, D. Skinner, G. Ceder, and K. A. Persson, Commentary: The materials project: A materials genome approach to accelerating materials innovation, *APL Materials* **1**, 011002 (2013).
 - [S21] P. Giannozzi, S. Baroni, N. Bonini, M. Calandra, R. Car, C. Cavazzoni, D. Ceresoli, G. L. Chiarotti, M. Cococcioni, I. Dabo, A. D. Corso, S. de Gironcoli, S. Fabris, G. Fratesi, R. Gebauer, U. Gerstmann, C. Gougoussis, A. Kokalj, M. Lazzeri, L. Martin-Samos, N. Marzari, F. Mauri, R. Mazzarello, S. Paolini, A. Pasquarello, L. Paulatto, C. Sbraccia, S. Scandolo, G. Sclauzero, A. P. Seitsonen, A. Smogunov, P. Umari, and R. M. Wentzcovitch, Quantum espresso: a modular and open-source software project for quantum simulations of materials, *Journal of Physics: Condensed Matter* **21**, 395502 (2009).
 - [S22] P. Giannozzi, O. Andreussi, T. Brumme, O. Bunau, M. B. Nardelli, M. Calandra, R. Car, C. Cavazzoni, D. Ceresoli, M. Cococcioni, N. Colonna, I. Carnimeo, A. D. Corso, S. de Gironcoli, P. Delugas, R. A. D. Jr, A. Ferretti, A. Floris, G. Fratesi, G. Fugallo, R. Gebauer, U. Gerstmann, F. Giustino, T. Gorni, J. Jia, M. Kawamura, H.-Y. Ko, A. Kokalj, E. Kkbenli, M. Lazzeri, M. Marsili, N. Marzari, F. Mauri, N. L. Nguyen, H.-V. Nguyen, A. O. de-la Roza, L. Paulatto, S. Ponc, D. Rocca, R. Sabatini, B. Santra, M. Schlipf, A. P. Seitsonen, A. Smogunov, I. Timrov, T. Thonhauser, P. Umari, N. Vast, X. Wu, and S. Baroni, Advanced capabilities for materials modelling with q uantum espresso, *Journal of Physics: Condensed Matter* **29**, 465901 (2017).
 - [S23] N. Marzari, D. Vanderbilt, A. De Vita, and M. C. Payne, Thermal contraction and disordering of the

- al(110) surface, *Phys. Rev. Lett.* **82**, 3296 (1999).
- [S24] H. J. Monkhorst and J. D. Pack, Special points for brillouin-zone integrations, *Phys. Rev. B* **13**, 5188 (1976).
- [S25] Thermo-pw:Ab-initio computation of material properties, https://dalcorsogithubio/thermo_pw/, accessed: 18.09.2019.